J. Iron Steel Res. Int. (2022) 29:1513–1525
https://doi.org/10.1007/s42243-022-00789-1

REVIEW

Review on niobium application in microalloyed steel

Lu-yan Sun[1,2] · Xiang Liu[3] · Xi Xu[3] · Shu-wei Lei[1,2] · Hui-gai Li[1,2] · Qi-jie Zhai[1,2]

Received: 10 December 2021 / Revised: 31 January 2022 / Accepted: 6 February 2022 / Published online: 24 May 2022

Abstract
With the rapid development of high-strength low-alloy (HSLA) steel, Nb as an important microalloying element has received more and more attention in recent years. The application and behavior of Nb in HSLA steel, including microstructures optimization, refining grain size, and precipitation behavior of Nb-containing phases, were reviewed. Nb could play an important role in following manners: (1) Nb-containing phases promote ferrite formation, and Nb solute promotes bainite formation. (2) Nb solute atoms and Nb-containing phases can inhibit the growth of austenite grains and austenite recrystallization. (3) Nb(C,N) that precipitates in ferrite/bainite can provide more significant strengthening contribution (more than 300 MPa) than that in austenite (about 100 MPa). Some reasonable suggestions for the production of Nb-bearing HSLA steel with excellent mechanical properties were put forward.

Keywords Niobium · Precipitate · Microalloying · High-strength low-alloy steel

1 Introduction

Microalloying technology appeared in the 1970s. High-strength low-alloy (HSLA) steels, often referred to as microalloyed (0.05–0.15 wt.%) steels, are low-carbon (usually < 0.2 wt.%) steels with the strength increased by small amounts of alloying elements such as niobium, vanadium, titanium, molybdenum, or boron, singly or in combination. Their tensile strength may reach 450 MPa, and their ductility may be as high as 30% [1–4]. The effects of microalloying are mainly related to microstructure refinement with respect to changes in the strengthening mechanisms: grain refinement strengthening, dislocation strengthening, solid solution strengthening, and dispersion strengthening [5, 6].

Nb, Ti, and V are the most common microalloying elements [7]. They can combine with C and N easily to form precipitates and then improve the strength and hardness of steel and also have the ability to optimize the microstructure [4]. In low-carbon steel, the strength increment produced by Nb microalloying is larger than that by Ti and V microalloying. Rancel et al. [8] found that the yield strength of the 0.019 wt.% Nb steel was slightly higher (about 30 MPa) than that of the experimental steel containing 0.038 wt.% Ti and much higher (about 80 MPa) than that of the 0.07 wt.% V steel, when the contents of other components were similar. In addition, niobium has superior economic advantage because of its abundant supply and stable price. Therefore, Nb is usually considered as a preferred microalloying element in HSLA steel.

Nb-bearing HSLA steel is mainly prepared by adding trace Nb to low-carbon steel or other HSLA steels [9, 10]. The effect of microalloying element Nb in HSLA steel depends on the state of Nb and the interaction between Nb and other solute elements or compounds. Nb exists in the HSLA steel mainly in the form of Nb solute or Nb-containing phases. In this paper, the application and behavior of Nb in HSLA steel are summarized and analyzed. Reasonable suggestions for optimizing microstructure, refining grain size, promoting the precipitation of Nb-containing phases, and improving properties are given.

✉ Hui-gai Li
lihuigai@i.shu.edu.cn

1 State Key Laboratory of Advanced Special Steel and Shanghai Key Laboratory of Advanced Ferrometallurgy and School of Materials Science and Engineering, Shanghai University, Shanghai 200444, China

2 Center for Advanced Solidification Technology (CAST), School of Materials Science and Engineering, Shanghai University, Shanghai 200444, China

3 Ansteel Group Iron and Steel Research Institute, Ansteel, Anshan, 114001, Liaoning, China

2 Microstructure optimization

One of the main functions of Nb microalloying is to optimize the room temperature microstructures [4, 11]. The effect of Nb on the phase transformation mainly depends on the state of Nb, as shown in Fig. 1.

Nb-containing phases can increase the transformation temperature and promote the austenite/ferrite transformation (Fig. 1). Ma et al. [12] found that the carbonitrides of Nb precipitated at austenite grain boundaries would provide heterogeneous nucleation sites to promote the nucleation of grain boundary ferrite, as shown in Fig. 2a. In addition, carbon near austenite grain boundaries is depleted when niobium combines with carbon and nitrogen to form carbonitrides, which decreases the local carbon concentration and promotes the formation of ferrite, as shown in Fig. 2b, c. Yuan et al. [13] found that compared with non-deformed Nb-bearing steel, the start temperature for austenite/ferrite transformation of hot deformed Nb-bearing steel increased by 110 °C at the cooling rate of 1 °C/s and by 40 °C at the cooling rate of 10 °C/s. The results showed that only at slow cooling rate can Nb precipitates nucleate and grow up to an appropriate size for heterogeneous nucleation of grain boundary ferrite. Yuan et al. [14] found that NbC in the size of 30–50 nm could offer ferrite nucleation sites. In addition, Nb(C,N) precipitated within austenite grains would form carbon-depleted zone around it, which promoted the formation of intragranular ferrite, as shown in Fig. 1. Chen et al. [15] found that before austenite/ferrite transformation, when the content of NbC precipitates increased from 54% to 62% and then to 87%, the microstructure would change from complete bainite to two-phase microstructures with different proportions of bainite and acicular ferrite, and finally to complete acicular ferrite, as shown in Fig. 3.

In contrast to the effect of Nb precipitates on austenite/ferrite transformation, Nb solute can increase the stability of supercooled austenite and decrease the transformation temperature [16], as shown in Fig. 1. The Nb solute would inhibit the grain boundary ferrite transformation and promote the bainite or martensite transformation [17, 18]. Okaguchi et al. [19] found that the start temperature for austenite/ferrite transformation decreased with increasing Nb content, as shown in Table 1. Yan and Bhadeshia [17] concluded that Nb solute atoms segregated to the austenite grain boundaries, which reduced the grain boundary energy of austenite and weakened the nucleation ability of ferrite. Hong et al. [20] concluded that the activity of carbon is reduced because of the strong interaction between Nb and C, which delayed the phase transformation.

Adjusting the state of Nb in a proper way can effectively optimize the microstructure. Carpenter and Killmore [21] found that different proportions of acicular ferrite and bainite could be obtained by adjusting Nb content and combining with high cooling rate (inhibiting the precipitation of Nb-containing phases) to increase the content of Nb solute, as shown in Fig. 4. At the cooling rate of 30 °C/s, the microstructure of Nb-free steel was mainly quasi-polygonal ferrite and a small amount of bainite, the microstructure of 0.024 wt.% Nb steel was mainly bainite, acicular ferrite and a handful of quasi-polygonal ferrite,

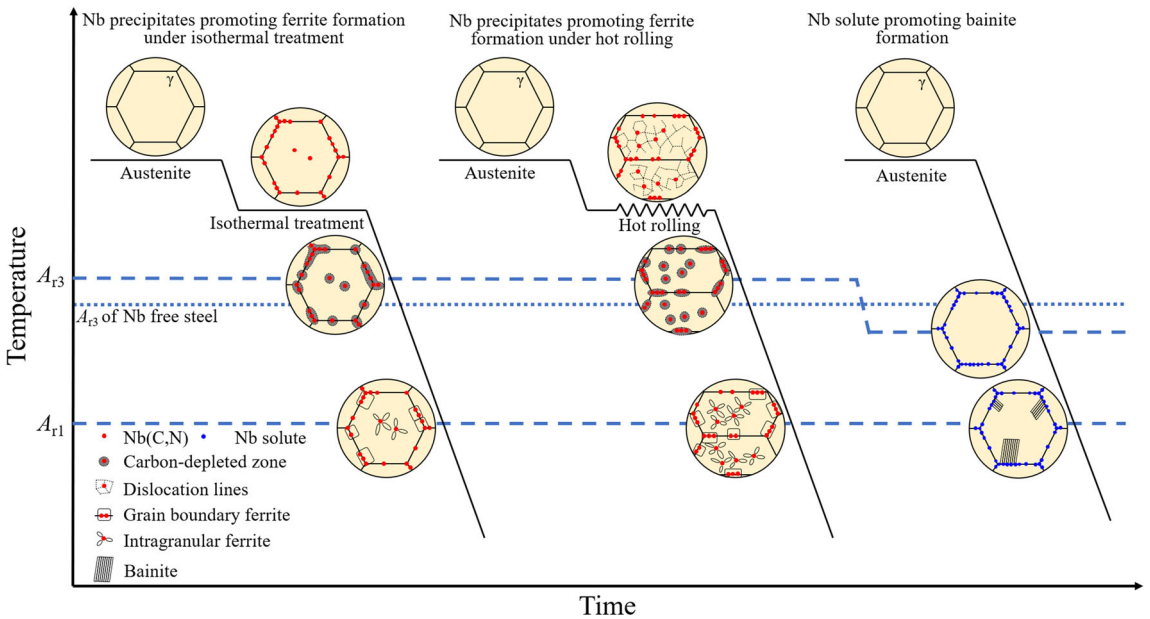

Fig. 1 Influence of Nb on phase transformation

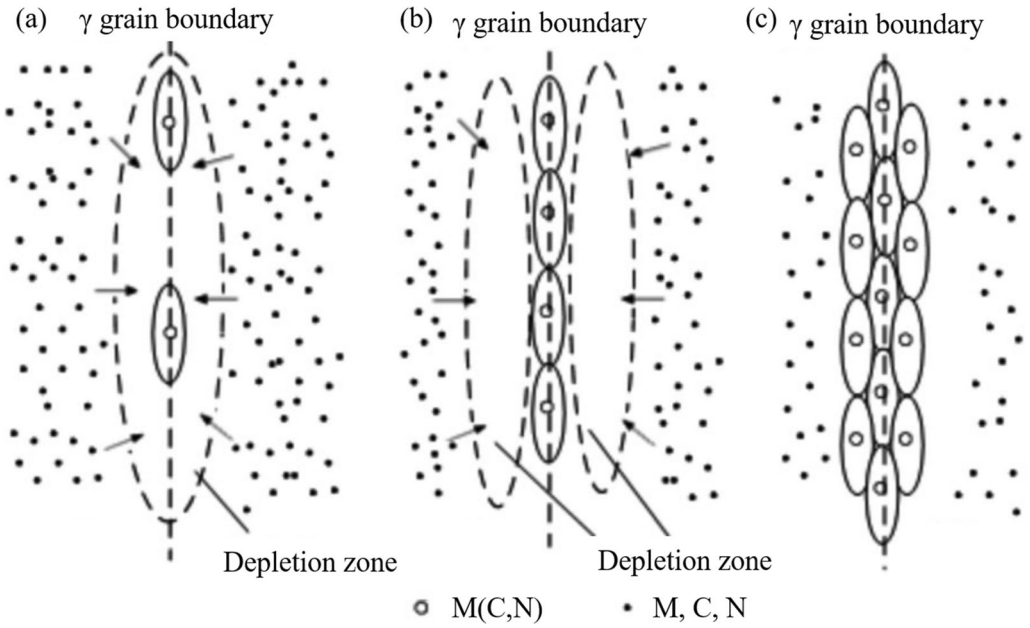

Fig. 2 Illustration of carbonitrides promoting formation of grain boundary ferrite [12]

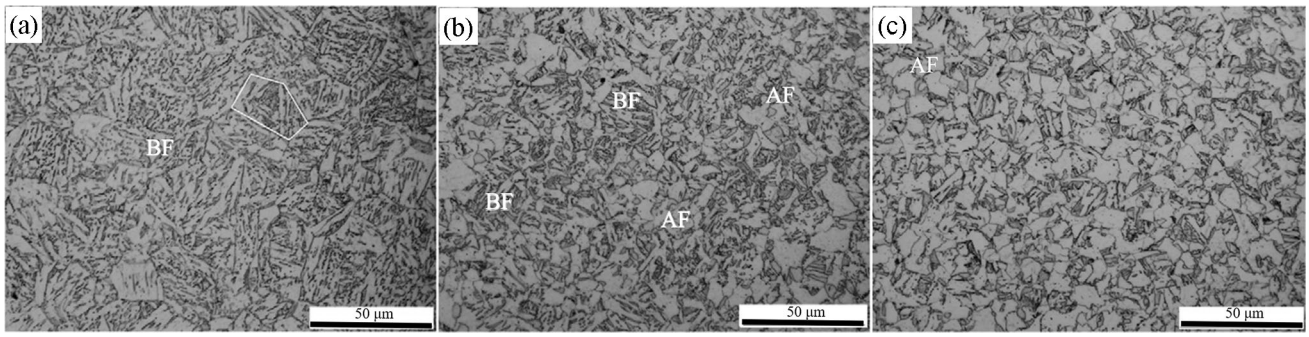

Fig. 3 Optical micrographs of specimens with different contents of Nb-containing phase. **a** 54% NbC; **b** 62% NbC; **c** 87% NbC. BF—Bainitic ferrite; AF—acicular ferrite [15]

Table 1 Austenite/ferrite transformation temperature of steels under different cooling rates and Nb contents [19]

Steel	C/wt.%	Si/wt.%	Mn/wt.%	Nb/wt.%	Cooling rate/(°C s^{-1})	A_{r3}/°C
1	0.10	0.24	1.49	–	5	739
3	0.10	0.26	1.50	0.02	5	719
5	0.10	0.26	1.50	0.04	5	701
2	0.10	0.24	1.49	–	10	680
4	0.10	0.26	1.50	0.02	10	646
6	0.10	0.26	1.50	0.04	10	628

and the microstructure of 0.06 wt.% Nb steel was bainite. Increasing the content of Nb solute promotes the formation of bainite. Bansal et al. [22] found that ferrite or pearlite formed during air cooling when Nb existed as precipitates in austenite, but bainite and some amount of grain boundary ferrite formed when Nb existed as a solute.

The aim of optimizing multi-phase microstructure is to enhance the combined property of steels [23, 24]. In a multi-phase steel, bainite contributes to the strength and

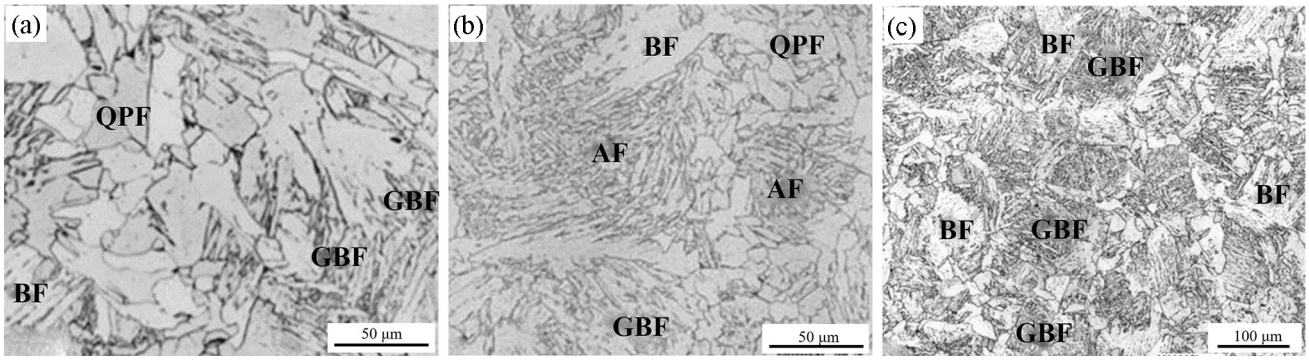

Fig. 4 Microstructure of low-carbon steels with different Nb contents at cooling rate of 30 °C/s. **a** 0 wt.% Nb; **b** 0.024 wt.% Nb; **c** 0.06 wt.% Nb. QPF—Quasi-polygonal ferrite; GBF—granular bainitic ferrite [21]

hardness of steel, while ferrite contributes to toughness and plasticity. The yield strength was about 1007 MPa for bainite and about 706 MPa for acicular ferrite in a fast-cooled low-carbon steel [25]. Although the yield strength of acicular ferrite is low, its three-dimensional interlocking shape can effectively inhibit crack propagation, which is beneficial to improve the plasticity and toughness [26–28]. Lan et al. [29] observed that a crack propagated straightly in bainite, but a crack terminated when it met with the acicular ferrite laths, as shown in Fig. 5. When the microstructure of steel was bainite, the total elongation was only 18.7%. The elongation would increase to 24.3% when containing acicular ferrite and bainite.

The cumulative contribution of different phases results in superior mechanical properties [30, 31]. Based on the above discussion and analysis, the ideal ratio of bainite and intragranular acicular ferrite multi-phase mixed microstructures can be obtained via the control of Nb in austenite and cooling rate. Bainite can ensure the overall strength and hardness of HSLA steel, and intragranular acicular ferrite can ensure toughness by inhibiting crack propagation.

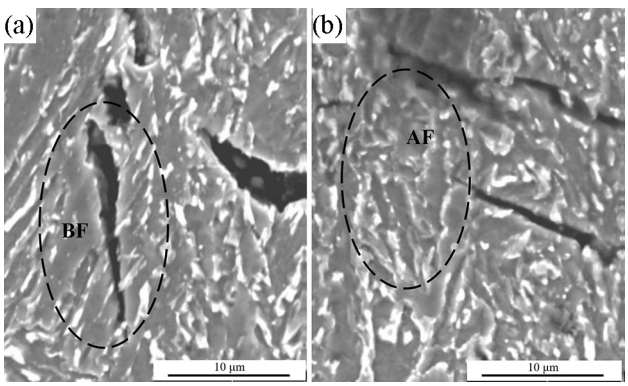

Fig. 5 Crack propagation in different microstructures. **a** Bainitic ferrite; **b** acicular ferrite [29]

3 Grain refinement

Refining grains size is the only way to improve both the strength and the toughness of steels [32]. Nb microalloying can play a good role in grain refinement in low-carbon steel, and its refining effect is the most significant among the three commonly used microalloying elements. The mechanism of the effect of Nb on grain refinement is summarized in Table 2.

In the austenitizing process, Nb can effectively inhibit the growth of austenite grains and increase the austenite grains coarsening temperature [33, 34]. Yuan et al. [13] found that the average size of austenite grains was refined from 248 to 69 μm with increasing Nb content when austenitizing temperature and time were the same (Fig. 6). The Nb precipitates pinning grain boundaries are one of the reasons for grain refinement during austenitizing process. The force of secondary phase to pin austenite grain boundaries is closely related to the secondary phase content. Dissolution of Nb precipitates will significantly increase the austenite grain size, because the pining force reduced [35, 36]. Zhang et al. [35] found that austenite grains grew up suddenly when the heating temperature was above 1050 °C, because the NbC precipitates began to dissolve (Fig. 7). Nb solute can also effectively inhibit the

Table 2 Phase and mechanism of Nb grain refinement

State of Nb	Mechanism	Affecting stage
Precipitates/solute (segregation)	Pinning grain boundaries	Austenitizing process
	Dragging grain boundaries	
Precipitates/solute (segregation)	Inhibiting austenite recrystallization	Recrystallization process
Precipitates	Nucleating cores for ferrite	Solid-state phase transformation

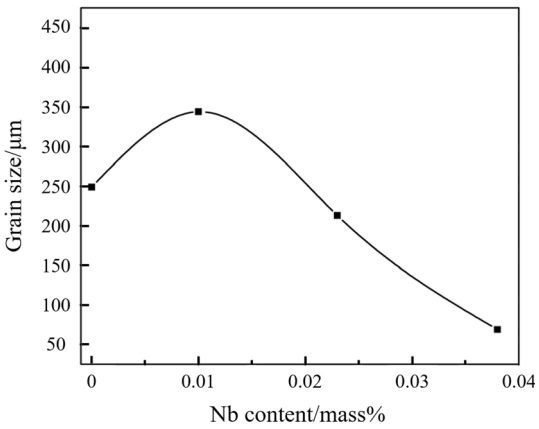

Fig. 6 Change of prior austenite grain size with Nb content [13]

growth of austenite grains through dragging mechanism. The atomic radius of Nb (0.1456 nm) is larger than that of Fe (0.1260 nm), and the dissolution of Nb atoms in Fe matrix will cause a large distortion energy. Grain boundary has many crystallographic defects, high energy, and loose atomic arrangement, and thus, the Nb atoms are easily concentrated here. This leads to a decrease in the energy of grain boundary, because solute atoms segregating at grain boundaries reduce the degree of disorder. Consequently, it is more difficult for grain boundaries to move away, and the mobility of the grain boundaries decreases. Felfer et al. [37] confirmed the obvious segregation of Nb atoms to the austenite grain boundaries using site-specific atom probe tomography. Yu et al. [38] found that Nb solute refined austenite grain size when austenitizing temperature was below 1230 °C in 0.015% Nb steel, but the austenite grain size was significantly coarsened when austenitizing temperature reached 1240 °C. McLean [39] proposed that there was a relationship between the concentration of solute atoms in grain boundaries (C_g) and the concentration of solute atoms in grains (C_0):

$$C_g = C_0 \exp\left(\frac{E}{RT}\right) \quad (1)$$

where R is the gas constant, R = 8.314 J/(mol K); T is the absolute temperature, K; and E is the distortion energy difference caused by solute atoms inside grain and at grain boundaries, J.

It can be seen that the level of atom segregation decreases with the increase in austenitizing temperature, leading to the increase in the mobility of grain boundaries. When the driving force of grain boundary movement is greater than the dragging force of Nb atoms, the grain boundary will quickly break away from the drag of atoms, resulting in the abnormal growth of austenite grains. In conclusion, both the mechanism of Nb-containing phases pinning grain boundary and Nb solute dragging grain boundary can effectively refine the austenite grain size within a certain range of austenitizing temperature. However, when the austenitizing temperature exceeds coarsening temperature, not only the Nb precipitates are dissolved, but also the segregation degree of Nb solute atoms at grain boundaries decreases, which leads to the sudden coarsening of austenite grains [40]. The abnormal growth of austenite grains will bring adverse effects on the properties of HSLA steel.

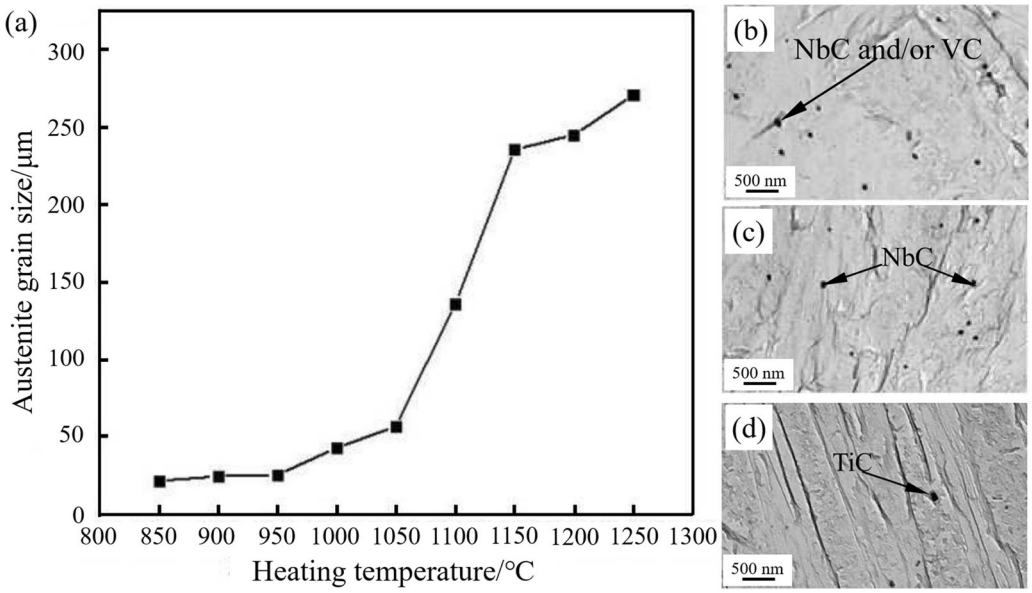

Fig. 7 Change in austenite grain size with austenitizing temperature (**a**) and precipitated phase at austenitizing temperature of 850 °C (**b**), 1150 °C (**c**), and 1250 °C (**d**) [35]

For deformed steel, Nb plays a significant role in grain refinement by inhibiting the recrystallization of deformed austenite and expanding the austenite non-recrystallization region [41–44]. Table 3 lists the inhibition rate of 1% major microalloying element solute atoms on the start time of austenite recrystallization at 900 °C. Nb is the most effective microalloying element to inhibit recrystallization [43]. Nb solute and Nb-containing phases can hinder the motion of grain boundaries, subgrain boundaries, and dislocations, which can effectively inhibit the nucleation of deformed austenite recrystallization. This can accumulate the deformation stress in austenite, and the accumulated stress acts as the driving force of austenite/ferrite transformation which increases the nucleation rate of ferrite and leads to the decrease in ferrite grain size [7, 45]. In addition, the inhibition of deformed austenite recrystallization allows the dislocation caused by thermal deformation to be preserved, and ferrite nucleates on the remaining dislocation, which helps to increase nucleation rate and refine grain size. Xie et al. [46] found that the addition of Nb suppressed the recrystallization of austenite so that the deformed austenite could be prevented from re-growing into equiaxed grains through recrystallization, which would make deformed austenite grains flat and fine, as shown in Fig. 8. This pancake-shape austenite can limit the growth of subsequent transformation products of austenite and refine the grain size [47].

In fact, Nb precipitates and Nb solute in deformed steel will play a role of grain refinement in different degrees. Some scholars considered that the dragging mechanism of Nb solute atoms plays a major role [48–52], while others thought that the pinning mechanism of Nb-containing phases plays a major role [53–56]. Xiao et al. [57] considered that Nb solute could more effectively retard dynamic recrystallization, while NbC precipitates are more effective to inhibit static recrystallization. The radius and electronegativity of solute atoms are the main factors affecting the mechanism of dragging grain boundaries. The larger the difference in the radius and electronegativity between alloying elements and Fe, the better the dragging effect. As shown in Table 3, the difference in radius and electronegativity between Nb and Fe is significant. The dragging effect of Nb is much better than that of other elements. Nb solute atoms have the best inhibitory effect on recrystallization.

The Nb-containing phases precipitated in austenite can be used as heterogeneous nucleation point of ferrite, which can increase the quantity density of ferrite and refine the ferrite grain size. Guo et al. [58] found that the amount of ferrite in Nb-bearing steel increased compared with Nb-free steel, and the ferrite grain size was refined from 2.38 to 1.90 μm, although the size of austenite grain of Nb-bearing steel was larger. Javaheri et al. [59] found that an addition of 0.013 wt.% Nb could refine the grain size of the final bainitic microstructures.

In conclusion, during austenitizing process, recrystallization and austenite/ferrite transformation, Nb-containing phases and Nb solute atoms have the effect of grain refinement. However, the austenitizing temperature and isothermal time should be reasonably designed to avoid the sudden growth of austenite grains in the process of austenitizing. In addition, both Nb precipitates and Nb solute can inhibit the recrystallization of deformed austenite and refine grain size in HSLA steel.

4 Precipitation strengthening

Same as grain refinement strengthening, the fine Nb precipitates can play a significant role in strengthening by hindering dislocation and grain boundary movement [60–63]. Compared with dislocation strengthening and solution strengthening, the brittleness vector of precipitation strengthening is lower. Nb is a strong carbide and nitride forming element and is easy to form Nb(C,N) in steel [64, 65]. According to the Orowan mechanism, the number and radius of Nb(C,N) have a significant influence on the effect of precipitation strengthening [66]. The larger the volume fraction of Nb precipitates, the smaller the radius, and the more significant the precipitation strengthening contribution.

Nb(C,N) can precipitate in three stages: in austenite matrix, during austenite/ferrite phase transformation, and in ferrite or bainite matrix, which will be discussed below.

Nb(C,N) precipitated in austenite has an orientation relationship with ferrite formed after austenite/ferrite

Table 3 Inhibition rate of 1% microalloying element solute atoms on start time of austenite recrystallization at 900 °C [43]

Solute	Fe	Ni	Cr	Mo	Nb	Ti	V
Radius/nm	0.126	0.124	0.127	0.139	0.145	0.146	0.134
Electronegativity	1.8	1.8	1.6	1.8	1.6	1.5	1.6
Inhibition rate/s	–	0.13	0.17	8.5	210	39	2.3

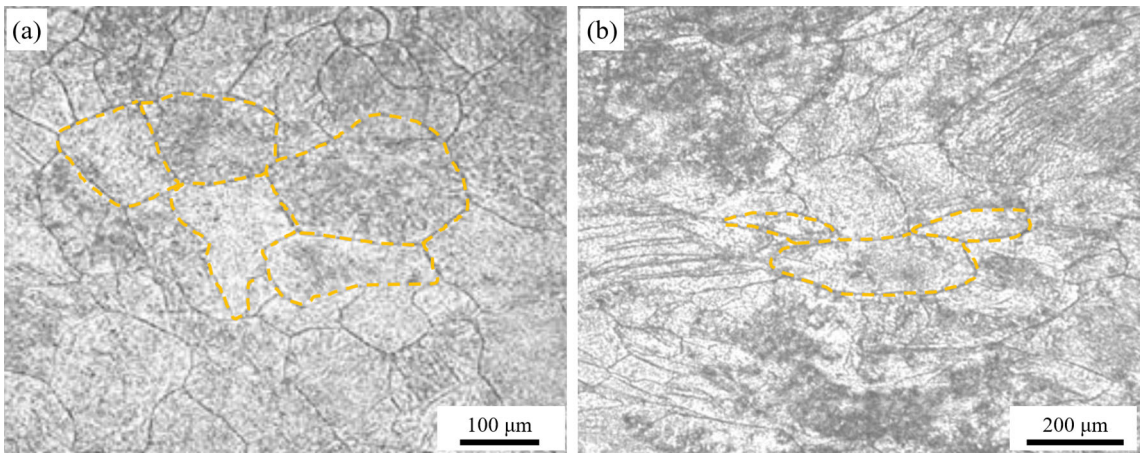

Fig. 8 Morphology of prior austenite in Nb-containing low-carbon steel under different hot rolling reductions. **a** 15% hot reduction; **b** 35% hot reduction [46]

transformation: $(111)_{Nb(C,N)}//(110)_{\alpha}$, $[110]_{Nb(C,N)}//[111]_{\alpha}$ (K-S relationship). Therefore, we can judge whether Nb(C,N) precipitates in austenite using the orientation relationship. In addition, the distribution of Nb(C,N) precipitated in austenite is also characteristic. Ma et al. [12] found that the segregation of Nb atoms would cause Nb(C,N) to precipitate mainly at austenite grain boundaries in non-hot-rolled low-carbon Nb-bearing steel. As shown in Fig. 9, Nb(C,N) aggregated with each other and distributed in chain along the austenite grain boundaries.

In 1968, Gray and Yeo [67] first discovered that Nb(C,N) precipitated at austenite/ferrite interface. The characteristic of this type of precipitation is that Nb-containing phases precipitate in line parallel to the phase transformation interface and have an orientation relationship with ferrite: $(100)_{Nb(C,N)}//(100)_{\alpha}$, $[010]_{Nb(C,N)}//[011]_{\alpha}$ (B-N relationship). The mechanism of interphase precipitation is that the solid solubility of Nb in ferrite is much lower than that in austenite. With the progress of phase transformation, Nb atoms accumulate near the phase transformation interface and combine with C which diffused from ferrite to austenite to form Nb precipitates. Li et al. [66] observed the interphase precipitated and randomly precipitated niobium carbides in an isothermally treated Nb-bearing steel (Fig. 10). The size and amounts of Nb(C,N) precipitated at transformation interface can be influenced by austenite/ferrite transformation temperature. The lower the temperature, the smaller the size and the higher the quantity density of Nb(C,N) [68]. With the decrease in austenite/ferrite transformation temperature, the driving force of Nb-containing phase precipitation increases, which increases the nucleation rate of the secondary phase, but the diffusion of Nb atoms is limited, which hinders the coarsening of Nb-containing phases. It is beneficial to obtain finer and denser Nb(C,N). Isothermal temperature and time also significantly affect Nb(C,N) precipitation at transformation interface. The lower isothermal temperature accelerates the austenite/ferrite phase transformation, thus speeding up the migration rate of the phase transformation interface and making it difficult for the secondary phases to nucleate and grow in a short time. In addition, in the initial stage of phase transformation, the speed of transformation is fast, and the mobility of interface is high, which make precipitation difficult to occur. In later stage of transformation, the mobility of interface decreases and Nb(C,N) precipitates. However, if the isothermal time is too short, precipitation will not occur during the transformation. The continuous cooling transformation (CCT) curve of ordinary microalloyed steel showed the isothermal temperature and time of Nb(C,N) interphase precipitation, random precipitation, and precipitation in bainite, as shown in Fig. 11 [56]. Funakawa et al. [69] found that the interphase precipitation of carbonitrides could provide strength contribution of nearly 300 MPa according to theoretical calculation. Li and Wang [70] used

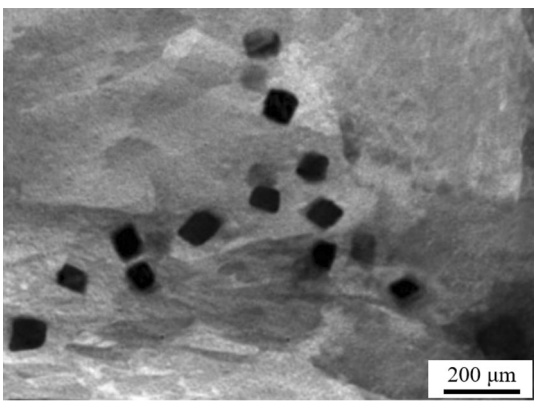

Fig. 9 Nanoscale Nb-containing secondary phases precipitated at austenite grain boundaries [12]

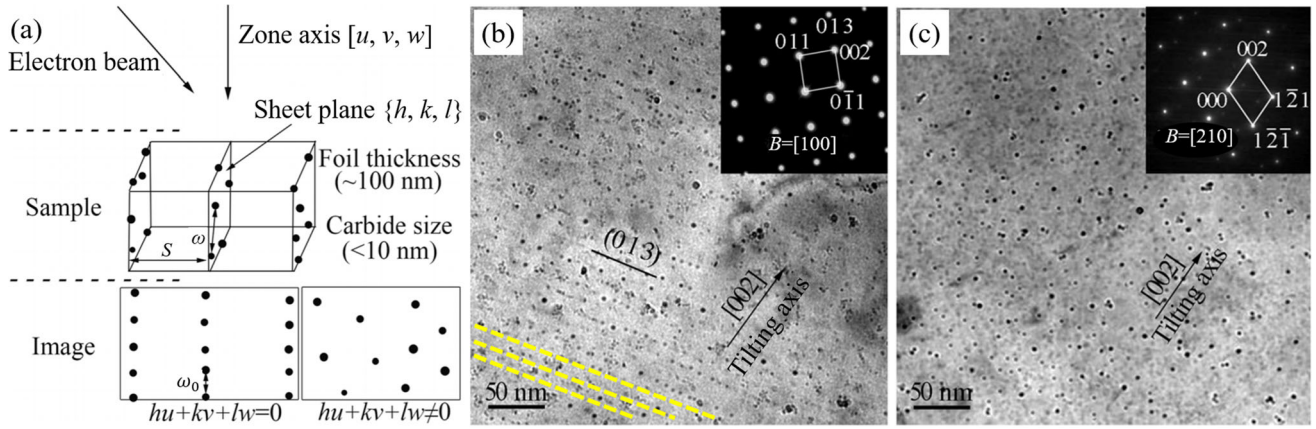

Fig. 10 Transmission electron microscopy (TEM) morphology of interphase precipitation and random dispersion of niobium carbides in specimen isothermally treated at 700 °C for 60 min. **a** Schematic of TEM observation about interphase precipitation of niobium carbide; **b** distribution of interphase precipitation of niobium carbides; **c** distribution of random dispersion of niobium carbides [66]

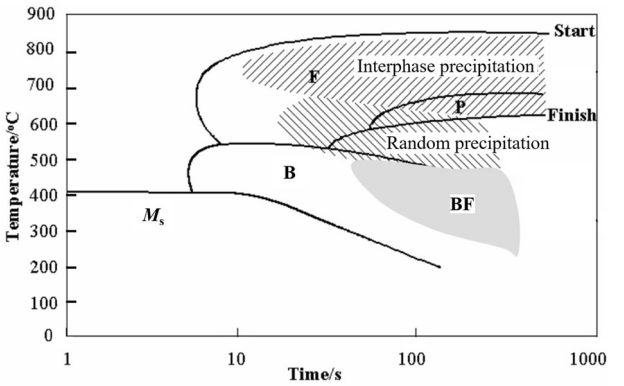

Fig. 11 CCT curve for microalloyed steel indicating approximate regions of interphase and random precipitation and precipitation in bainitic ferrite. B—Bainite; F—ferrite; P—pearlite [56]

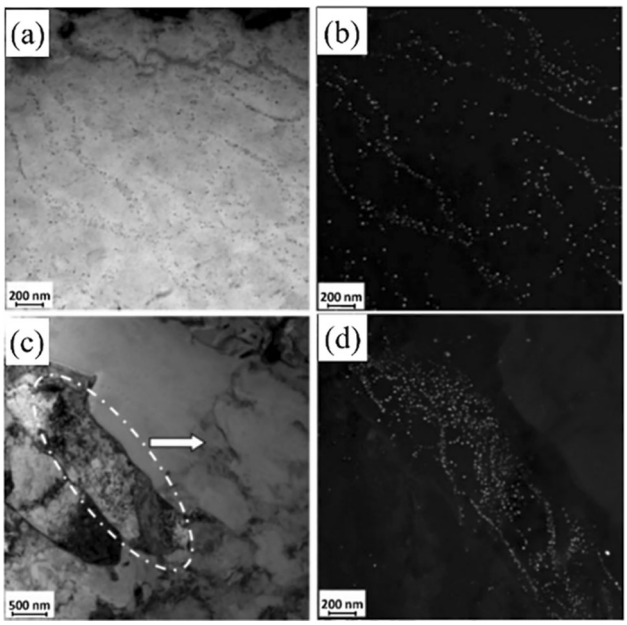

Fig. 12 Bright and dark field images of precipitate. **a**, **b** Ferrite; **c**, **d** bainite [73]

Orowan mechanism to calculate and found that the precipitation strengthening increment of interphase precipitation was more than 300 MPa and the maximum reached 475 MPa. It can be seen that the interphase precipitation of Nb(C,N) can provide considerable strength contribution.

The supersaturated precipitation of Nb(C,N) in ferrite or bainite has a B-N orientation relationship with ferrite, which is in accordance with the relationship between Nb(C,N) precipitation at transformation interface and ferrite. Nb(C,N) precipitated in austenite is independent of the matrix at room temperature, while Nb(C,N) precipitated in ferrite can combine well with matrix, which can provide more significant strengthening contribution [71]. Wang [72] found that Nb(C,N) precipitated in austenite would be coarsened as steel was cooled to room temperature because the solute atoms had more time to diffuse at high temperature, which weakened the contribution of precipitation strengthening. Wang et al. [73] found that the size of Nb(C,N) precipitated in bainite was smaller than that in ferrite, and the amount was greater as well, as shown in Fig. 12. The reason is related to the shear mechanism of bainite transformation. The bainite transformation does not consume the defects in the original austenite, and additional defects are generated due to volume expansion, which will promote the nucleation of Nb(C,N) and increase the nucleation rate of Nb(C,N). Park and Lee [74] measured the precipitation kinetics of Nb(C,N) using resistivity method and confirmed that Nb(C,N) precipitated only after the completion of bainite transformation.

Nb mainly plays the role of grain refinement strengthening and precipitation strengthening in microalloyed steel, but does not play the full role in precipitation strengthening owing to the limitation of solid solution of Nb in austenite

[75, 76]. The maximum use of Nb in HSLA steel depends on understanding the relationship among processing parameters, precipitation thermodynamics, and precipitation dynamics [77]. The factors influencing the precipitation behavior of Nb(C,N) are as follows.

(1) Composition of steel
The addition of Si can increase the activity of C and N and increase the driving force of Nb(C,N) precipitation. B can increase the diffusion coefficient of Nb in austenite and the vacancy density in matrix, which can accelerate Nb(C,N) nucleation. Mn has the opposite effect. Mn increases the solid solubility product of Nb(C,N) in austenite and reduces the diffusivity of Nb, which weakens the precipitation trend of Nb(C,N). Mo, Cr, Ni, and V also have the same inhibitory effect [78, 79]. Zhang et al. [80] found that the (Nb,Mo)C in Nb–Mo-bearing steel has higher coarsening resistance than NbC in Nb-bearing steel. On one hand, Mo can reduce the interface energy between carbide and austenite. On the other hand, the addition of Mo reduces the diffusivity of Nb atoms. Therefore, Mo is beneficial to refining the size of Nb(C,N) [81, 82]. The addition of Ti promotes the heterogeneous nucleation of Nb(C,N) [83–85]. Ti-containing inclusions can act as heterogeneous nucleation sites for Nb(C,N) to form composite inclusions which are usually large in size and difficult to dissolve when reheated [86, 87]. Gong et al. [88] found that Ti could reduce the dissolution rate of Nb-containing phase during reheating. Rare earth elements also have significant effect on the precipitation behavior of Nb-containing phases [89–91]. In austenite, rare earth elements can extend the incubation period of Nb(C,N) precipitation, reduce the precipitation rate, inhibit the precipitation of Nb(C,N) and improve the solid solubility of Nb. Geng et al. [92] found that adding rare earth can increase the solid solution content of Nb by 54% at the austenitizing temperature of 1250 °C. In ferrite, rare earth elements can increase the precipitation rate of Nb(C,N) and make Nb(C,N) smaller in size and more in quantity. In summary, Ti, Si, and B contribute to the precipitation of Nb(C,N), but Mn, V, Mo, Cr, and Ni inhibit the precipitation. Specifically, rare earth elements inhibit the precipitation of Nb(C,N) in austenite, yet they help Nb(C,N) precipitation in ferrite.

(2) Controlled rolling and controlled cooling
Engineers often use the controlled rolling and controlled cooling to improve the strength, toughness, and weldability of HSLA steel [93–95]. Nb(C,N) usually precipitates at grain boundaries in Nb-microalloyed steels due to solute segregation. After hot rolling treatment, the dislocations introduced by hot deformation will replace grain boundaries as the preferential nucleation points of Nb(C,N) [96]. Studies have shown that the existence of dislocations will increase the diffusion rate of Nb, C, and N atoms, leading to significantly accelerated nucleation, growth, and coarsening of the precipitates [7]. Pereloma et al. [42] found that reducing hot rolling temperature increased the amount of Nb-containing phases precipitated in austenite, thus reducing the amount of Nb-containing phases precipitated in ferrite and weakening the effect of precipitation strengthening. Kostryzhev et al. [97] found that the amount of Nb-containing phases that precipitated during the phase transformation and in ferrite decreased with the decrease in deformation temperature. The time when Nb(C,N) begins to precipitate in deformed steel is three orders of magnitude faster than that in undeformed steel, and the quantity density of Nb(C,N) in deformed steel is also much higher than that in undeformed steel [98]. The cooling rate can affect the precipitation behavior of Nb(C,N) during continuous cooling. Nb(C,N) was easy to coarsen at slow cooling rate [99]. However, too fast cooling rate would inhibit the precipitation of Nb-containing phases [100]. The quantity density of Nb(C,N) decreased significantly at fast cooling rate (Fig. 13).

(3) Isothermal treatment parameters
In order to obtain a good combination of strength and toughness, tempering process is widely used after thermo-mechanical treatment [101]. Nanoscale Nb-containing phases can precipitate during the isothermal process and provide precipitation strengthening [102]. Park et al. [103] found that Nb(C,N) size increased from 5.7 to 18.9 nm as the isothermal temperature increased from 850 to 950 °C. At 900 °C, the size of Nb(C,N) increased from 7.8 to 14.1 nm when the isothermal time increased from 120 to 300 s. According to the Orowan mechanism, the increase in size of secondary phases means that the effect of precipitation strengthening is weakened. Therefore, it is necessary to determine the appropriate isothermal temperature and time according to the composition of the Nb-bearing steel to avoid the precipitates coarsening and ensure the strength contribution. There is a certain isothermal temperature that makes the smallest size and the largest quantity of Nb-containing phases. The size of Nb-containing phases would increase with the increase in isothermal time [104]. Xie et al. [105] found that the average size of nanoscale NbC

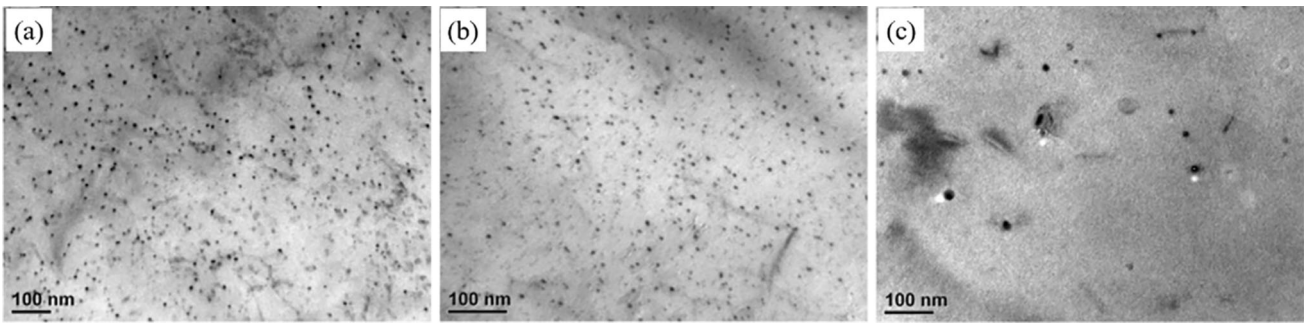

Fig. 13 TEM morphology of (Nb,Ti)C secondary phase in Ti–Nb–Mo low-carbon steel at different cooling rates. **a** 0.5 °C/s; **b** 1 °C/s; **c** 5 °C/s [99]

was 4.1–6.1 nm when steel was isothermally tempered at 550–680 °C and the yield strength was increased by 86–173 MPa.

Finally, the influence of controlled rolling and controlled cooling parameters and isothermal treatment parameters on the size, volume fraction, and precipitation location of Nb-containing phases and the contribution of precipitation to the increment of yield strength are also summarized in Table 4.

From Group A in Table 4, we can see that hot rolling contributes to the enhancement of the yield strength of steel due to the size refinement of Nb(C,N) because of dislocation accumulation caused by hot rolling. From Group B and C in Table 4, we can find an optimum option for either isothermal time or isothermal temperature. The size decrease of Nb(C,N) contributes more to the yield strength of steel than the volume fraction increase of Nb(C,N). This can be explained using the Orowan formula [107]: $\sigma = \frac{0.8MGb}{\sqrt{\frac{2}{3}}\left(\sqrt{\frac{\pi}{f}}-2\right)r}$, where σ is the yield strength of steel; M is the Taylor factor; G is the shear modulus of elasticity; b is the Burgers vector; f is the volume fraction; and r is the radius of Nb-containing phases. The yield strength of steel is inversely proportional to the radius of Nb(C,N) and is proportional to the square root of the volume fraction of Nb(C,N). From Group D in Table 4, we can see that the increase in cooling rate contributes to the enhancement in the yield strength of steel due to the obvious size refinement of Nb(C,N).

5 Summary

Nb-microalloyed steels have both high strength and high ductility with optimized complex microstructures. Increasing the solid solubility of Nb in steel, controlling the state of Nb in austenite, and promoting the precipitation of Nb-containing phases in ferrite or austenite are reliable techniques to improve steel properties.

1. The addition of Nb in HSLA steel can optimize microstructure. Nb solute promotes the formation of bainite with high strength, and Nb-rich phases promote the formation of intragranular ferrite with high plasticity and toughness. In addition, the ratio of two phases can be adjusted by changing the content of Nb and the existence mode of Nb so as to achieve the most balanced combination of strength and toughness.
2. Both Nb solute and Nb-rich phase can play a significant role in grain refinement during thermo-mechanical treatment. However, the austenitizing temperature and time should be reasonably determined according to the content of Nb in the austenitizing process to avoid the abnormal growth of austenite grains. Controlled rolling can be combined with the inhibition of recrystallization by Nb microalloying to retain dislocation and strain energy in austenite and then improve nucleation rate and refine grain size.
3. The precipitation of nanoscale Nb(C,N) can improve the strength of HSLA steel by precipitation strengthening. The supersaturated precipitation of Nb(C,N) in ferrite or bainite can be promoted by adjusting the process parameters of thermo-mechanical treatment and isothermal annealing.

6 Future trends

With the expansion of product types and the improvement of production technology, the addition of Nb in steel is attracting more and more attention. In the early days, Nb was used for grain refinement and precipitation strengthening in steels with ferrite–pearlite structure. Now, due to the pursuit of higher strength, bainite and martensite become the target structures. In order to make maximum use of Nb element in steel, the characteristics of the

Table 4 Effect of heat treatment on Nb-containing phase and strength of steel

Group	Composition	Heat treatment	Parameters of influencing factors	Nb-containing phases		Precipitation site	Contribution on yield strength of steel/MPa
				Diameter/nm	Volume fraction/%		
A	0.08%C–0.038%Nb [103]	Austenitizing for 600 s at 1250 °C	Isothermal holding for 120 s at 900 °C	14.8	0.39	Austenite grain boundaries	102
			Two-pass hot rolling at 1150 °C and isothermal holding for 120 s at 900 °C	7.8	0.36	Dislocation in austenite (main) and grain boundaries	156
B	0.08%C–0.038% Nb [103]	Austenitizing for 600 s at 1250 °C, two-pass hot rolling at 1150 °C	Isothermal holding for 300 s at 850 °C	5.7	0.15	Dislocation in austenite (main) and grain boundaries	125
			Isothermal holding for 300 s at 900 °C	14.1	0.8	Dislocation in austenite (main) and grain boundaries	151
			Isothermal holding for 300 s at 950 °C	18.9	0.4	Dislocation in austenite (main) and grain boundaries	85
C	0.09%C–0.025%Nb [66]	Austenitizing for 300 s at 1200 °C	Isothermal holding for 10 min at 650 °C	3.26	0.0207	Ferrite	80
			Isothermal holding for 20 min at 650 °C	4.15	0.0483	Ferrite	110
			Isothermal holding for 60 min at 650 °C	6.29	0.0917	Ferrite	104
D	0.07%C–0.02%Nb [106]	Austenitizing for 120 min at 1250 °C, three-pass hot rolling at 1050 °C, four-pass hot rolling at 880 °C	Cooling to room temperature at 0.5 °C/s	30	0.042	Ferrite, pearlite	52
			Cooling to 650 °C at 80 °C/s, and cooling to room temperature at 0.5 °C/s	3.5	0.213	Ferrite, pearlite	247

microalloyed steel must be predicted, and the composition and production process must be carefully designed. Research efforts also need to be put on the accurate simulation about the effect of Nb on phase transformation, grain refinement, and precipitation strengthening of steel under different compositions and processes.

References

[1] J.G. Lenard, Elsevier Science, Waterloo, Ontario, CAN, 2014, pp. 163–191.
[2] K.Y. Xie, T.X. Zheng, J.M. Cairney, H. Kaul, J.G. Williams, F.J. Barbaro, C.R. Killmore, S.P. Ringer, Scripta Mater. 66 (2012) 710–713.
[3] Q. Yuan, G. Xu, S. Liu, M. Liu, H.J. Hu, G.Q. Li, Metals 8 (2018) 518.
[4] F.Z. Bu, X.M. Wang, S.W. Yang, C.J. Shang, R.D.K. Misra, Mater. Sci. Eng. A 620 (2015) 22–29.
[5] T.P. Wang, F.H. Kao, S.H. Wang, J.R. Yang, C.Y. Huang, H.R. Chen, Mater. Lett. 65 (2011) 396–399.
[6] J. Chen, F. Li, Z.Y. Liu, S. Tang, G.D. Wang, ISIJ Int. 53 (2013) 1070–1075.
[7] B. Dutta, E.J. Palmiere, C.M. Sellars, Acta Mater. 49 (2001) 785–794.
[8] L. Rancel, M. Gómez, S.F. Medina, Steel Res. Int. 79 (2008) 947–953.
[9] C.M. Yang, Y.S. Hu, Y.D. Xin, J. Peng, Iron Steel Vanadium Titanium 20 (1999) No. 1, 27–31.
[10] W.L. Gao, Y. Leng, D.F. Fu, J. Teng, Mater. Des. 105 (2016) 114–123.
[11] R. Hou, G. Xu, H.J. Hu, M.X. Zhou, Metallogr. Microstruct. Anal. 6 (2017) 158–163.
[12] F.J. Ma, G.H. Wen, W.L. Wang, Steel Res. Int. 84 (2013) 370–376.
[13] X.Q. Yuan, Z.Y. Liu, S.H. Jiao, L.Q. Ma, G.D. Wang, ISIJ Int. 46 (2006) 579–585.
[14] X.Q. Yuan, Z.Y. Liu, S.H. Jiao, X.H. Liu, G.D. Wang, ISIJ Int. 47 (2007) 1658–1665.
[15] Y. Chen, D.T. Zhang, Y.C. Liu, H.J. Li, D.K. Xu, Mater. Charact. 84 (2013) 232–239.
[16] T. Jia, M. Militzer, Metall. Mater. Trans. A 46 (2015) 614–621.
[17] P. Yan, H.K.D.H. Bhadeshia, Mater. Sci. Technol. 31 (2015) 1066–1076.
[18] P. Cizek, B.P. Wynne, C.H.J. Davies, B.C. Muddle, P.D. Hodgson, Metall. Mater. Trans. A 33 (2002) 1331–1349.
[19] S. Okaguchi, T. Hashimoto, H. Ohtani, in: International Conference on Physical Metallurgy of Thermomechanical Processing of Steels and Other Metals, Iron and Steel Institute of Japan, Tokyo, Japan, 1988, pp. 330–336.
[20] S.C. Hong, S.H. Lim, H.S. Hong, K.J. Lee, D.H. Shin, K.S. Lee, Mater. Sci. Eng. A 355 (2003) 241–248.
[21] K.R. Carpenter, C.R. Killmore, Metals 5 (2015) 1857–1877.
[22] G.K. Bansal, V.C. Srivastava, S.G. Chowdhury, Mater. Sci. Eng. A 767 (2019) 138416.
[23] Y.C. Liu, L. Shi, C.X. Liu, L.M. Yu, Z.S. Yan, H.J. Li, Mater. Sci. Eng. A 675 (2016) 371–378.
[24] X.H. Li, Y.C. Liu, K.F. Gan, J. Dong, C.X. Liu, Mater. Sci. Eng. A 785 (2020) 139350.
[25] H.T. Xiao, S.B. Zheng, Y. Xin, J.L. Xu, K. Han, H.G. Li, Q.J. Zhai, Metals. 10 (2020) 995.
[26] D.E.C. Van, O. Grong, J. Hjelen, in: Proceedings of the International Conference on Solid-Solid Phase Transformations, Solid-Solid Phase Transformation, Kyoto, Japan, 1999, pp. 78–85.
[27] Y. Shao, C.X. Liu, Z.S. Yan, H.J. Li, Y.C. Liu, J. Mater. Sci. Technol. 34 (2018) 737–744.
[28] W.L. Costin, O. Lavigne, A. Kotousov, Mater. Sci. Eng. A 663 (2016) 193–203.
[29] H.F. Lan, L.X. Du, R.D.K. Misra, Mater. Sci. Eng. A 611 (2014) 194–200.
[30] W.J. Nie, X.M. Wang, S.J. Wu, H.L. Guan, C.J. Shang, Sci. China Technol. Sci. 55 (2012) 1791–1796.
[31] J.Z. Xue, Z.Z. Zhao, D. Tang, H. Li, H.H. Wu, W.L. Xiong, L. Liang, Y. Huang, J. Iron Steel Res. Int. 28 (2020) 346–359.
[32] J.Y. Tian, G. Xu, W.C. Liang, Q. Yuan, Metallogr. Microstruct. Anal. 6 (2017) 233–239.
[33] E.J. Palmiere, C.I. Garcia, A.J. De Ardo, Metall. Mater. Trans. A 25 (1994) 277–286.
[34] X. Liu, F. Zhao, Z.Q. Dong, C.L. Zhang, Y.S. Kou, Y.Z. Liu, Mater. Sci. Forum 817 (2015) 121–126.
[35] L.C. Zhang, X.L. Wen, Y.Z. Liu, Mater. Sci. Forum 898 (2017) 783–790.
[36] Y. Zhang, X.H. Li, Y.C. Liu, C.X. Liu, J. Dong, L.M. Yu, H.J. Li, Mater. Charact. 169 (2020) 110612.
[37] P.J. Felfer, C.R. Killmore, J.G. Williams, K.R. Carpenter, S.P. Ringer, J.M. Cairney, Acta Mater. 60 (2012) 5049–5055.
[38] Q.B. Yu, Z.B. Zhang, Z.L. Li, X. Wei, Iron and Steel 41 (2006) No. 12, 70–74.
[39] D. McLean, Can. Metall. Quart. 13 (1974) 145–153.
[40] B.Y. Yan, Y.C. Liu, Z.J. Wang, C.X. Liu, Y.H. Si, H.J. Li, J.X. Yu, Materials 10 (2017) 1017.
[41] S.N. Prasad, D.S. Sarma, Mater. Sci. Eng. A 408 (2005) 53–63.
[42] E.V. Pereloma, A.G. Kostryzhev, A. AlShahrani, C. Zhu, J.M. Cairney, C.R. Killmore, S.P. Ringer, Scripta Mater. 75 (2014) 74–77.
[43] Q.B. Yu, Z.D. Wang, X.H. Liu, G.D. Wang, Mater. Sci. Eng. A 379 (2004) 384–390.
[44] A. Karmakar, S. Biswas, S. Mukherjee, D. Chakrabarti, V. Kumar, Mater. Sci. Eng. A 690 (2017) 158–169.
[45] M. Gomez, P. Valles, S.F. Medina, Mater. Sci. Eng. A 528 (2011) 4761–4773.
[46] K.Y. Xie, L. Yao, C. Zhu, J.M. Cairney, C.R. Killmore, F.J. Barbaro, J.G. Williams, S.P. Ringer, Metall. Mater. Trans. A 42 (2011) 2199–2206.
[47] L.Z. Chang, X.F. Shi, L. Zhou, J.J. Wang, Adv. Mater. Res. 476–478 (2012) 205–211.
[48] C.W. Sinclair, C.R. Hutchinson, Y. Bréchet, Metall. Mater. Trans. A 38 (2007) 821–830.
[49] M. Hillert, B. Sundman, Acta Metall. 24 (1976) 731–743.
[50] R. Kirchheim, Acta Mater. 50 (2002) 413–419.
[51] C.L. Miao, C.J. Shang, H.S. Zurob, G.D. Zhang, S.V. Subramanian, Metall. Mater. Trans. A 43 (2012) 665–676.
[52] A. Varshney, S. Sangal, S. Kundu, K. Mondal, Mater. Des. 95 (2016) 75–88.
[53] C.R. Hutchinson, H.S. Zurob, C.W. Sinclair, Y.J.M. Brechet, Scripta Mater. 59 (2008) 635–637.
[54] H.S. Zurob, G. Zhu, S.V. Subramanian, G.R. Purdy, C.R. Hutchinson, Y. Brechet, ISIJ Int. 45 (2005) 713–722.
[55] S. Vervynckt, K. Verbeken, P. Thibaux, Y. Houbaert, Mater. Sci. Eng. A 528 (2011) 5519–5528.
[56] S. Zajac, Mater. Sci. Forum 500–501 (2005) 75–86.
[57] F.R. Xiao, Y.B. Cao, G.Y. Qiao, X.B. Zhang, B. Liao, J. Iron Steel Res. Int. 19 (2012) No. 11, 52–56.
[58] S.Z. Guo, W.Y. Yang, G.A. Chen, Z.Q. Sun, J. Univ. Sci. Technol. Beijing 29 (2007) 586–590.

[59] V. Javaheri, N. Khodaie, A. Kaijalainen, D. Porter, Mater. Charact. 142 (2018) 295–308.
[60] T. Dorin, K. Wood, A. Taylor, P. Hodgson, N. Stanford, Mater. Charact. 112 (2016) 259–268.
[61] G.A. Chen, W.Y. Yang, S.Z. Guo, Z.Q. Sun, Mater. Sci. Forum 475–479 (2005) 105–108.
[62] A. Grajcar, J. Therm. Anal. Calorim. 118 (2014) 1011–1020.
[63] T. Niu, Y.L. Kang, H.W. Gu, Y.Q. Yin, M.L. Qiao, J. Iron Steel Res. Int. 17 (2010) No. 11, 73–78.
[64] Y.P. Ma, X.L. Li, Y.G. Liu, S.Y. Zhou, X.M. Dang, China Foundry 9 (2012) 148–153.
[65] J.C. Zhang, T. Zhang, Y.T. Yang, J. Iron Steel Res. Int. 28 (2020) 739–751.
[66] X.L. Li, C.S. Lei, X.T. Deng, Y.M. Li, Y. Tian, Z.D. Wang, G.D. Wang, Acta Metall. Sin. (Engl. Lett.) 30 (2017) 1067–1079.
[67] J.M. Gray, R.B.G. Yeo, ASM Trans. 61 (1968) 255–269.
[68] S.S. Nayak, R.D.K. Misra, J. Hartmann, F. Siciliano, J.M. Gray, Mater. Sci. Eng. A 494 (2008) 456–463.
[69] Y. Funakawa, T. Shiozaki, K. Tomita, T. Yamamoto, E. Maeda, ISIJ Int. 44 (2004) 1945–1951.
[70] X.L. Li, Z.D. Wang, Acta Metall. Sin. 51 (2015) 417–424.
[71] M. Charleux, W.J. Poole, M. Militzer, A. Deschamps, Metall. Mater. Trans. A 32 (2001) 1635–1647.
[72] G.D. Wang, Steel Rolling 29 (2012) No. 1, 1–8.
[73] X.N. Wang, Y.F. Zhao, B.J. Liang, L.X. Du, H.S. Di, Steel Res. Int. 84 (2013) 402–409.
[74] J.S. Park, Y.K. Lee, Scripta Mater. 57 (2007) 109–112.
[75] T. Furuhara, K. Kikumoto, H. Saito, T. Sekine, T. Ogawa, S. Morito, T. Maki, ISIJ Int. 48 (2008) 1038–1045.
[76] E.S. Siradj, Mater. Sci. Forum 1000 (2020) 404–411.
[77] A.C. e Silva, Calphad 68 (2020) 101720.
[78] F. Siciliano Jr., J.J. Jonas, Metall. Mater. Trans. A 31 (2000) 511–530.
[79] F. Siciliano, E.I. Poliak, Mater. Sci. Forum 500–501 (2005) 195–202.
[80] Z.Y. Zhang, X.J. Sun, Z.Q. Wang, Z.D. Li, Q.L. Yong, G.D. Wang, Mater. Lett. 159 (2015) 249–252.
[81] H.L. Andrade, M.G. Akben, J.J. Jonas, Metall. Trans. A 14 (1983) 1967–1977.
[82] W.B. Lee, S.G. Hong, C.G. Park, K.H. Kim, S.H. Park, Scripta Mater. 43 (2000) 319–324.
[83] J.G. Jung, E. Shin, Y.K. Lee, Metall. Mater. Trans. A 48 (2017) 76–85.
[84] Y. Lee, B.C. De Cooman, ISIJ Int. 54 (2014) 893–899.
[85] M. Kapoor, R. O'Malley, G.B. Thompson, Metall. Mater. Trans. A 47 (2016) 1984–1995.
[86] J. Webel, A. Herges, D. Britz, E. Detemple, V. Flaxa, H. Mohrbacher, F. Mücklich, Metals 10 (2020) 243.
[87] J.M. Zhang, W.H. Sun, H. Sun, J. Iron Steel Res. Int. 17 (2010) No. 10, 63–67.
[88] P. Gong, E.J. Palmiere, W.M. Rainforth, Acta Mater. 97 (2015) 392–403.
[89] C.L. Li, Chinese Rare Earths 34 (2013) No. 3, 78–85.
[90] Q. Lin, B.W. Chen, L. Tang, L.S. Li, X.Y. Zhu, H.B. Wang, J. Rare Earth 21 (2003) 167–171.
[91] H.Y. Wang, X.Y. Gao, W.M. Mao, G.H. Zhu, S.M. Chen, H.P. Ren, ISIJ Int. 56 (2016) 1646–1651.
[92] K.K. Geng, Q. Fang, Y. Dong, Z.L. Jin, Heat Treat. Met. 41 (2016) No. 1, 106–110.
[93] A. Ghosh, S. Das, S. Chatterjee, B. Mishra, P.R. Rao, Mater. Sci. Eng. A 348 (2003) 299–308.
[94] M.C. Zhao, K. Yang, Y.Y. Shan, Mater. Sci. Eng. A 335 (2002) 14–20.
[95] R. González, J.O. García, M.A. Barbés, M.J. Quintana, L.F. Verdeja, J.I. Verdeja, J. Iron Steel Res. Int. 17 (2010) No. 10, 50–56.
[96] S. Okaguchi, T. Hashimoto, ISIJ Int. 32 (1992) 283–290.
[97] A.G. Kostryzhev, A.A. Shahrani, C. Zhu, J.M. Cairney, S.P. Ringer, C.R. Killmore, E.V. Pereloma, Mater. Sci. Eng. A 607 (2014) 226–235.
[98] I. Dutta, D.L. Bourell, Acta Metall. Mater. 38 (1990) 2041–2049.
[99] F.Z. Bu, X.M. Wang, L. Chen, S.W. Yang, C.J. Shang, R.D.K. Misra, Mater. Charact. 102 (2015) 146–155.
[100] S.F. Medina, A. Quispe, M. Gomez, Metall. Mater. Trans. A 45 (2014) 1524–1539.
[101] Q. Yuan, G. Xu, J.Y. Tian, W.C. Liang, Arab. J. Sci. Eng. 42 (2017) 4771–4777.
[102] Z. Li, D.H. Wen, Y. Ma, Q. Wang, G.Q. Chen, R.Q. Zhang, R. Tang, H. He, J. Iron Steel Res. Int. 25 (2018) 717–723.
[103] J.S. Park, Y.S. Ha, S.J. Lee, Y.K. Lee, Metall. Mater. Trans. A 40 (2009) 560–568.
[104] X.L. Li, Z.D. Wang, X.T. Deng, Y.M. Li, H.N. Lou, G.D. Wang, Mater. Lett. 182 (2016) 6–9.
[105] Z.J. Xie, X.P. Ma, C.J. Shang, X.M. Wang, S.V. Subramanian, Mater. Sci. Eng. A 641 (2015) 37–44.
[106] X.T. Deng, T.L. Fu, Z.D. Wang, G.H. Liu, G.D. Wang, R.D.K. Misra, Met. Mater. Int. 23 (2017) 175–183.
[107] N. Kamikawa, K. Sato, G. Miyamoto, M. Murayama, N. Sekido, K. Tsuzaki, T. Furuhara, Acta Mater. 83 (2015) 383–396.